International Journal of Minerals, Metallurgy and Materials
Volume 24, Number 10, October 2017, Page 1183
DOI: 10.1007/s12613-017-1509-z

Hydrogen storage properties of MgH_2 co-catalyzed by LaH_3 and NbH

Jian-zheng Song[1,2], *Zi-yang Zhao*[2], *Xin Zhao*[2], *Rui-dong Fu*[1], *and Shu-min Han*[1,2]

1) State Key Laboratory of Metastable Materials Science and Technology, Yanshan University, Qinhuangdao 066004, China

2) College of Environmental and Chemical Engineering, Yanshan University, Qinhuangdao 066004, China

(Received: 30 December 2016; revised: 3 May 2017; accepted: 4 May 2017)

Abstract: To improve the hydrogen storage properties of Mg-based alloys, a composite material of MgH_2 + 10wt%LaH_3 + 10wt%NbH was prepared by a mechanical milling method. The composite exhibited favorable hydrogen desorption properties, releasing 0.67wt% H_2 within 20 min at 548 K, which was ascribed to the co-catalytic effect of LaH_3 and NbH upon dehydriding of MgH_2. By contrast, pure MgH_2, an MgH_2 + 20wt%LaH_3 composite, and an MgH_2 + 20wt%NbH composite only released 0.1wt%, 0.28wt%, and 0.57wt% H_2, respectively, under the same conditions. Analyses by X-ray diffraction and scanning electron microscopy showed that the composite particle size was small. Energy-dispersive X-ray spectroscopic mapping demonstrated that La and Nb were distributed homogeneously in the matrix. Differential thermal analysis revealed that the dehydriding peak temperature of the MgH_2 + 10wt%LaH_3 + 10wt%NbH composite was 595.03 K, which was 94.26 K lower than that of pure MgH_2. The introduction of LaH_3 and NbH was beneficial to the hydrogen storage performance of MgH_2.

Keywords: energy storage materials; hydrogen absorbing materials; mechanical milling; phase transformation; activation analysis

1. Introduction

In recent years, new energy resources have been eagerly sought because fossil fuels are being gradually exhausted and their combustion products pollute our environment [1–2]. Hydrogen, with the advantages of not being a pollutant or generating pollutants through combustion, having a high energy density, and being naturally abundant, is considered an ideal energy carrier [3–4]. However, hydrogen storage is a major challenge. Storing hydrogen in some solid materials via physical or chemical adsorption is more promising than storing hydrogen in high-pressure containers or as a liquid. Metal hydrides that provide high hydrogen storage capacity have been studied as promising materials over the past several decades. Magnesium hydride (MgH_2) is a material with strong hydrogen storage potential because of its high hydrogen storage capacity (7.6wt%), low density, good reversibility, and low cost [5–8]. However, its practical application is currently unfeasible because of its inferior kinetics and high thermodynamic stability (ΔH = −74.6 kJ·mol^{-1} H_2) [9–11].

Enormous efforts have been made to ameliorate the hydriding/dehydriding properties of MgH_2. Among them, reducing particle size by high-energy mechanical milling [12–13] and compositing MgH_2 with additives such as transition metals [14–15], metal oxides [16–17], metal halides [18–19], and rare-earth metals [20–21] have been reported to be two important methods. The hydriding/dehydriding characteristics of MgH_2 were improved dramatically after ball milling with Ti, Fe, and Ni, which was ascribed to the co-catalysis of these three metals [22–23]. Recently, Mg-based transition-metal complex hydrides Mg_2FeH_6@MgH_2 and hierarchical structure catalysts (Fe/C, Co/C, and Ni/C) were designed and fabricated to overcome the agglomeration issue of nanocatalysts [24–25]. In addition to hierarchical-structured catalysts, MAX-phase Ti_3AlC_2 or Ti_3C_2 compounds with layers have also been reported to improve the dehydriding properties of MgH_2 by catalyzing effects [26–27]. Meanwhile, some Mg-based hydrides with a special crystal structure were considered to show excellent dehydriding properties. More recently, a β-/γ-MgH_2 nanocomposite with enhanced hydrogen desorption kinetics was synthesized via a simple wet chemical route [28–29].

Rare-earth metals and their hydrides are widely used as

Corresponding author: Shu-min Han E-mail: hanshm@ysu.edu.cn

high-efficiency catalysts for Mg-based hydrogen storage materials. Composite materials MgH_2 + 20wt%LaH_3 and $LiBH_4$−Mg_2NiH_4 + 10wt%$CeH_{2.29}$ exhibited a faster absorption/desorption process and a higher hydrogen absorption/desorption capacity [30–31]. Recently, Nb and Nb_2O_5 have also been widely used to improve the hydrogen absorption and desorption kinetics of MgH_2. Conceição *et al*. [32] reported that metallic niobium and niobium oxides with a high surface area could markedly enhance the hydrogen absorption and desorption kinetics of MgH_2. Their MgH_2 + 5wt%s-Nb_2O_5 sample absorbed 5.2wt% of hydrogen within 1.3 min at 300°C. Jin *et al*. [33] investigated the hydrogen absorption and desorption performances of MgH_2 with Nb hydride obtained by alloying MgH_2 with 1mol% NbF_5. They illustrated that the formation of NbH was essential in catalyzing the hydrogen storage of MgH_2. The NbH-catalyzed MgH_2 desorbed 6.3wt% H_2 in 15 min and absorbed more than 90% of its initial hydrogen capacity within 5 min at 573 K. Zhang *et al*. [34] found that a more disordered structure and smaller particle size of NbH*x* resulted in a better catalytic effect on the hydrogen storage performance of MgH_2.

As previously discussed, both the La hydride and the Nb hydride can improve the hydriding and dehydriding properties of Mg-based hydrides. Therefore, to enhance the hydriding/dehydriding kinetics and decrease the decomposition temperature of MgH_2, we prepared a novel LaH_3 and NbH co-doped MgH_2 composite by mechanical milling and subsequently investigated the catalytic effects of LaH_3 and NbH on the hydrogen desorption of an Mg-based hydride in detail.

2. Experimental

The original materials—MgH_2 powder (purity > 98%), lanthanum powder (purity > 99.9%), and Nb powder (purity > 99.5%), were purchased from Alfa-Aesar. The LaH_3 was obtained by hydrogenating the La powder under 5.0-MPa H_2 pressure for 5 h at 723 K. The NbH was obtained by hydrogenating the Nb powder under 4.5 MPa of H_2 pressure at 623 K for 1 h using equipment designed to measure pressure–composition–temperature (P–C–T) characteristics. Previous experiments on the kinetics properties of MgH_2 milled with different amounts of LaH_3 demonstrated that MgH_2 ball milled with 20wt% LaH_3 exhibited the best performance. Thus, 2.0 g of MgH_2 powder, together with 20wt% NbH, 10wt%LaH_3 + 10wt%NbH, and 20wt% LaH_3 and without additives, was ball-milled under an Ar atmosphere for 5 h using a QM-ISP2 planetary mill at a speed of 500 r·min^{-1} (the obtained composites were designated as MgH_2–NbH, MgH_2–NbH–LaH_3, MgH_2–LaH_3, and pure MgH_2). The mass ratio of ball-to-powder was 30:1. All of the experimental operations were conducted in an Ar-filled (99.99% purity) glove box to prevent oxidation of the samples.

Phase analysis of the samples after mechanical milling, after hydrogenation at 623 K for 2 h, and after dehydrogenation at 623 K for 2 h was performed by X-ray diffraction (XRD) on a D/MAX-2500/PC diffractometer equipped with a Cu K_α radiation source. Microstructure observations were carried out by scanning electron microscopy (SEM) on a HITACHI S-4800 electron microscope equipped with an energy-dispersive X-ray spectrometer. Hydriding/dehydriding properties of the samples were measured using the P–C–T instrument. The hydriding processes at 473 and 523 K were conducted under an initial hydrogen pressure of 3 MPa, and the dehydriding process was carried out at 548 K under an initial hydrogen pressure of 0.1 MPa. To fit the activation energy to the Kissinger equation, the dehydriding peak temperature of the hydrogenated samples were detected using a simultaneous thermal analyzer (DTG-60A) with the samples under Ar protection; the analysis was conducted from 300 to 773 K at heating rates of 5, 10, 15, and 20 K·min^{-1}.

3. Results and discussion

3.1. Microstructures

Fig. 1 presents the XRD pattern of the Nb metal powder hydrogenated under 4.5 MPa of H_2 pressure at 623 K for 1 h. As shown in Fig. 1, NbH peaks are well fitted to the standard peak positions of NbH and no Nb peaks are observed. Thus, NbH was successfully prepared. The preparation of LaH_3 was described in our previous work [22]. The obtained LaH_3 and NbH were used as precursors in the subsequent experiments.

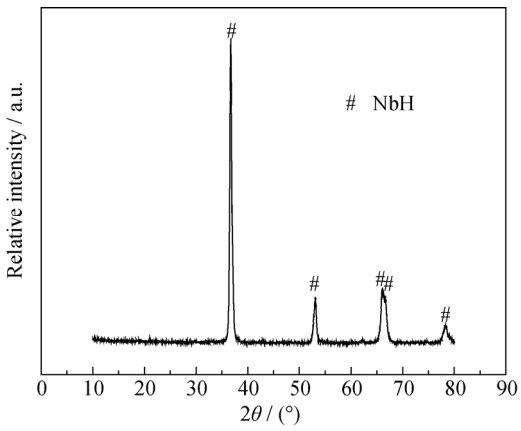

Fig. 1. XRD pattern of the Nb metal powder after hydrogenation.

Fig. 2 presents the XRD patterns of MgH_2–NbH at three different treatment stages (after ball milling, after hydrogenation, and after dehydrogenation). Fig. 2(a) indicates that the ball-milled MgH_2–NbH is composed of an MgH_2 phase and an NbH phase. The wide diffraction peaks of the sample indicate that small hydride nanocrystals were obtained during the mechanical milling process. Such small nanocrystals offer more surface area for the hydrogenation and dehydrogenation processes. Fig. 2(b) shows the XRD pattern of MgH_2–NbH hydride hydrogenated at 623 K for 2 h at the fourth hydriding/dehydriding cycle. The main phases are also MgH_2 and NbH, similar to the main phases of the ball-milled sample. However, the diffraction peaks are sharper than those in the pattern of the ball-milled sample, demonstrating the formation of a hydride with high crystallinity during the hydrogenation process. Moreover, some diffraction peaks absent in the pattern of the ball-milled sample are observed in the pattern of the hydrogenated sample, indicating the formation of a new phase. As shown in Fig. 2(c), after dehydrogenation at 623 K for 2 h, the MgH_2 phase is transformed into an Mg phase, whereas the NbH remains stable, implying that the NbH phase plays a catalytic role.

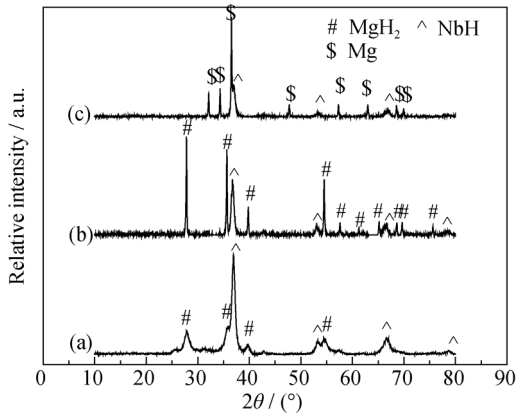

Fig. 2. XRD patterns of MgH_2–NbH: (a) ball-milled; (b) after hydrogenation at 623 K for 2 h; (c) after dehydrogenation at 623 K for 2 h.

The XRD patterns of the MgH_2–LaH_3 sample before and after dehydrogenation have been discussed in our previous work [30]. The MgH_2 phase and LaH_3 phase were detected in the dehydrogenated sample, indicating that the dehydrogenation was not complete. Moreover, the XRD patterns indicate that the LaH_3 phase partially transformed into the $LaH_{2.3}$ phase during the dehydriding process. The phase transition from the LaH_3 phase to the $LaH_{2.3}$ phase caused an obvious volume contraction and resulted in a distinct strain of MgH_2, which can improve its hydrogenation and dehydrogenation properties.

The XRD patterns of the MgH_2–NbH–LaH_3 composite are presented in Fig. 3. As shown in Fig. 3(a), the as-milled sample is composed of an MgH_2 phase, an LaH_3 phase, and a small amount of NbH phase. Fig. 3(b) shows that the hydrogenated MgH_2–NbH–LaH_3 also consists of an MgH_2 phase, an LaH_3 phase, and a small amount of NbH phase. The diffraction peaks become sharper and some small peaks become more prominent because of crystallization at 623 K under the H_2 atmosphere. Moreover, the NbH phase appears after hydrogenation. Fig. 3(c) shows that the main phases of the dehydrogenated sample are an Mg phase and the $LaH_{2.3}$ phase, consistent with the phases observed after hydrogenation of the MgH_2–LaH_3 sample. However, the peaks of the NbH phase partly overlap those of the Mg phase. Collectively, these results indicate that the MgH_2 phase transformed into the Mg phase, the LaH_3 phase transformed into the $LaH_{2.3}$ phase, and the NbH phase remained stable.

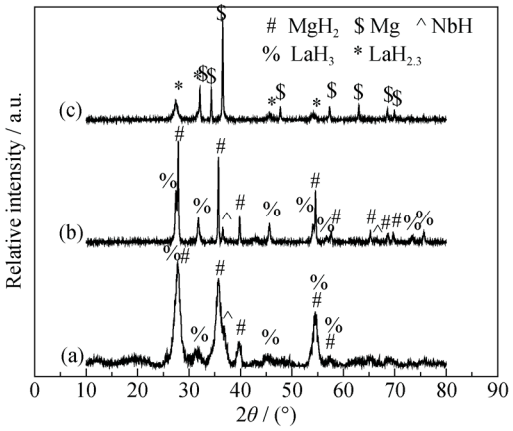

Fig. 3. XRD patterns of MgH_2–NbH–LaH_3: (a) ball-milled; (b) after hydrogenation at 623 K for 2 h; (c) after dehydrogenation at 623 K for 2 h.

The different phase transformation processes of MgH_2–NbH, MgH_2–LaH_3, and MgH_2–NbH–LaH_3 composites demonstrate that NbH and LaH_3 play different roles in the hydrogenation and dehydrogenation processes. The LaH_3 mainly manipulates the structure of the hydride, whereas NbH acts as the catalyst. The synergistic effect of LaH_3 and NbH is expected to improve the hydrogenation and dehydrogenation performance of the MgH_2–NbH–LaH_3 composite.

Scanning electron micrographs of the dehydrogenated MgH_2–NbH, MgH_2–NbH–LaH_3, and MgH_2–LaH_3 samples are shown in Fig. 4. Fig. 4(a) shows that the particles of MgH_2–NbH are uniform in size, ranging from 0.5 to 1 μm. The MgH_2–NbH–LaH_3 composite exhibits a particle size similar to that of the MgH_2–NbH composite, but its particles

are slightly agglomerated (Fig. 4(b)). However, in the case of the MgH_2–LaH_3 composite, the agglomeration is more severe and the agglomerates are much larger. Therefore, we deduced that MgH_2–NbH and MgH_2–NbH–LaH_3 possess smaller particle sizes and higher specific surface areas than the MgH_2–LaH composite, which is beneficial to the hydriding/dehydriding kinetics of MgH_2.

To investigate the elemental distribution in MgH_2–NbH–LaH_3, EDS maps were collected; the results are presented in Fig. 5. Fig. 5(a) shows an SEM micrograph of the analyzed area. Figs. 5(b)–5(d) show the distribution of Mg, Nb, and La, respectively. Mg is mainly distributed in the aggregated particles, whereas Nb and La are uniformly distributed over the whole samples. This result indicates that NbH and LaH_3 prevent aggregation of the hydride. Moreover, the well-distributed Nb and La particles among the Mg particles can provide additional channels and shorten the diffusion length of hydrogen atoms.

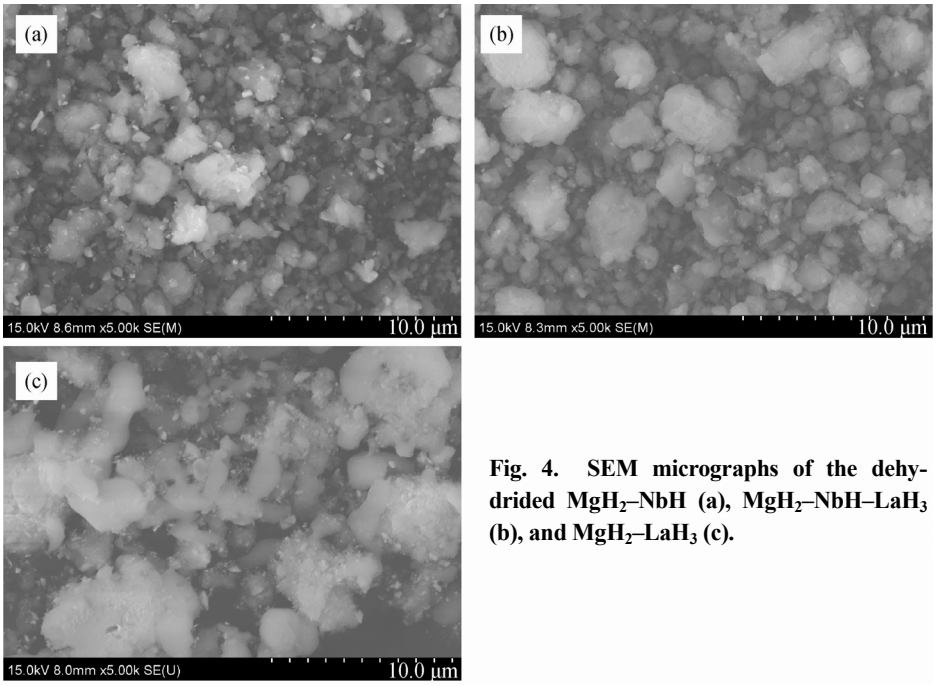

Fig. 4. SEM micrographs of the dehydrided MgH_2–NbH (a), MgH_2–NbH–LaH_3 (b), and MgH_2–LaH_3 (c).

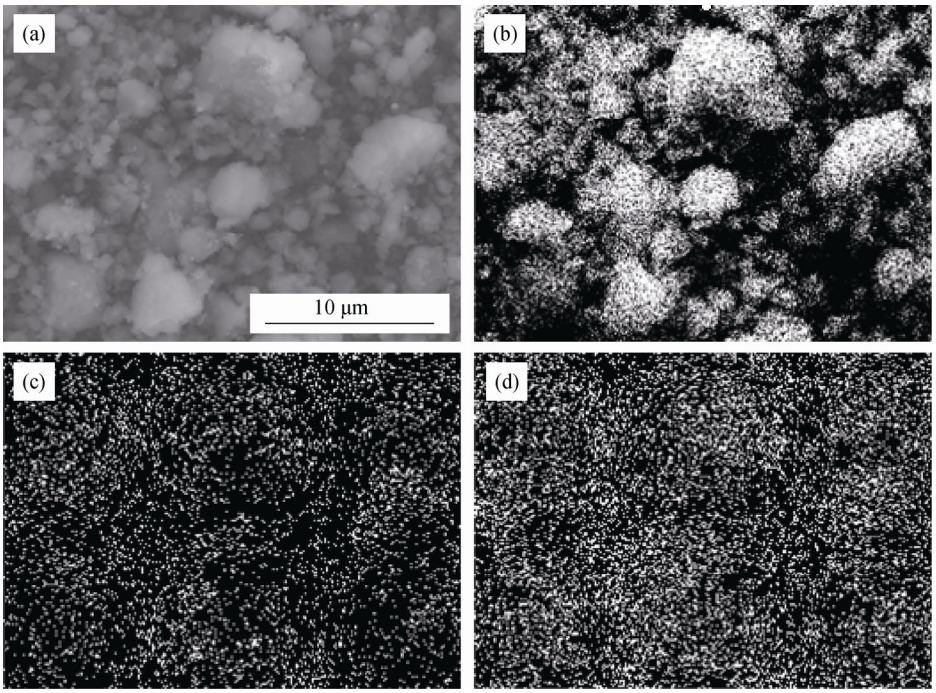

Fig. 5. BF-SEM image (a) and EDS maps showing the distribution of Mg (b), Nb (c), and La (d) in MgH_2–NbH–LaH_3.

3.2. Hydrogen absorption/desorption properties

The hydrogen absorption curves of MgH_2–NbH, MgH_2–NbH–LaH_3, MgH_2–LaH_3, and pure MgH_2 at 523 and 473 K are shown in Fig. 6. The hydrogenation data were recorded at the fourth hydrogen absorption/desorption cycle at 623 K under a hydrogen pressure of 3 MPa. Fig. 6(a) shows that the MgH_2–NbH composite exhibits the highest hydrogen absorption rate and absorbs 5.30wt% H_2 within 3 min. The MgH_2–NbH–LaH_3 and MgH_2–LaH_3 composites absorb 4.73wt% and 3.98wt% H_2, respectively, under the same conditions. By contrast, pure MgH_2 absorbs only 2.37wt% H_2 within 3 min. From Fig. 6(b), the hydrogen absorption capacity of MgH_2–NbH, MgH_2–NbH–LaH_3, and MgH_2–LaH_3 composites are 4.87wt%, 4.11wt%, and 2.78wt%, respectively, within 3 min. However, the sample of pure MgH_2 only absorbs 0.53wt% H_2 within the same time. These results clearly indicate that MgH_2 catalyzed by NbH, LaH_3, and LaH_3 + NbH performs much better than pure MgH_2 in both maximum hydrogen storage capacity and hydrogen absorption rate.

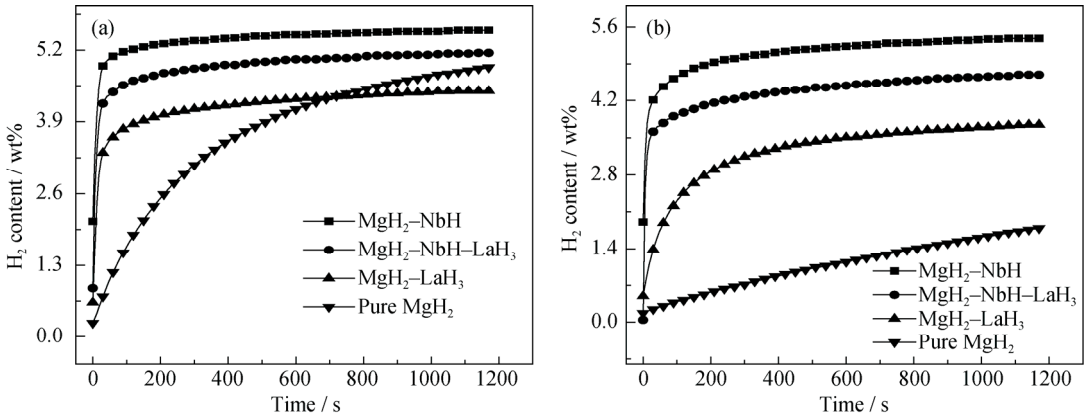

Fig. 6. Hydriding curves of MgH_2–NbH, MgH_2–NbH–LaH_3, MgH_2–LaH_3, and pure MgH_2: (a) 523 K; (b) 473 K.

The reaction mechanism during the hydrogen absorption process can be investigated by comparing the observed hydriding rate with the predictions of certain kinetics equations. The hydrogenation process is well fitted to the Avrami–Erofeev equation (Eq. (1)):

$$\alpha = 1 - e^{-kt^m} \quad (1)$$

where α is the reacted fraction versus time t, k is the rate constant, and m is the order of the reaction.

As shown in Fig. 7, the fitted lines almost coincide with the practical experimental data, indicating that the hydrogen absorption processes of MgH_2–NbH and MgH_2–NbH–LaH_3 at 523 K are well accordant with the Avrami–Erofeev equation. The two composites follow the reaction mechanism of nucleation and growth. The k values for MgH_2–NbH and MgH_2–NbH–LaH_3 are 0.915 and 0.695, respectively. Zhu *et al*. [30] found that the hydrogen adsorption behaviors of an MgH_2 + 20wt%LaH_3 composite and MgH_2 were also well fitted using the Avrami–Erofeev equation and that the k values of the two samples were 0.282 and 0.00734, respectively. The k value represents the rate of hydrogen absorption reaction. It explains why MgH_2–NbH exhibits the fastest hydrogen absorption rate, as revealed by the hydriding curves, among the investigated composite materials.

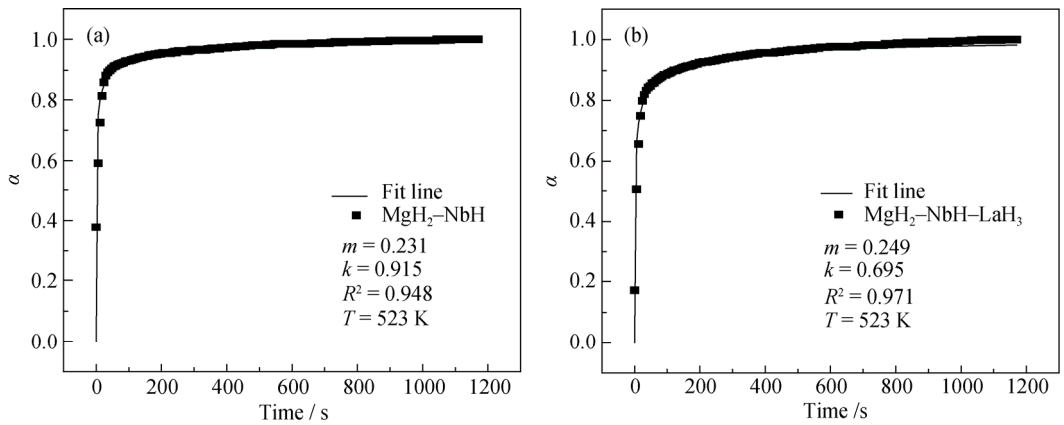

Fig. 7. Fitted hydrogenation kinetics curves for MgH_2–NbH (a) and MgH_2–NbH–LaH_3 (b) at 523 K.

In Fig. 8, the fitted lines for MgH_2–NbH, MgH_2–NbH–LaH_3, and MgH_2–LaH_3 at 473 K agree well with the experimental results, indicating that the hydriding process of the three samples accord with the reaction mechanism of nucleation and growth. However, in Fig. 8(a), the fitted line for pure MgH_2 is not consistent with the experimental data, which is ascribed to a change in the reaction mechanism of pure MgH_2 at 473 K.

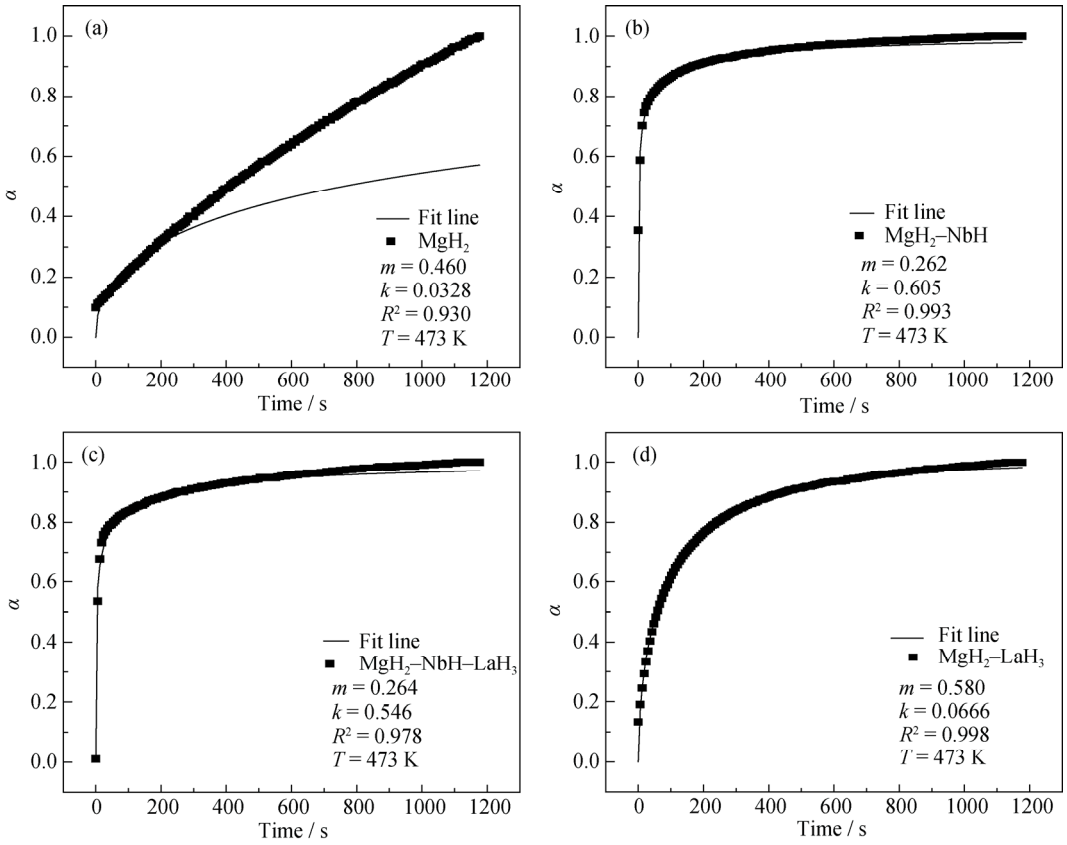

Fig. 8. Fitted hydrogenation kinetics curves for pure MgH_2 (a), MgH_2–NbH (b), MgH_2–NbH–LaH_3 (c), and MgH_2–LaH_3 (d) at 473 K.

The MgH_2–NbH, MgH_2–NbH–LaH_3, and MgH_2–LaH_3 composites can not only improve the hydrogen absorption performance of MgH_2 but also enhance its dehydrogenation behavior. As shown in Fig. 9, the MgH_2–NbH–LaH_3 composite released 0.67wt% H_2 within 20 min at 548 K, more than twice that released by MgH_2–LaH_3. Under the same conditions, MgH_2–NbH released 0.57wt% H_2 and the pure MgH_2 released only approximately 0.1wt% H_2. The dehydriding curves indicate that the additive composed of LaH_3 and NbH is more effective in improving the dehydriding kinetics of MgH_2, which is attributed to the co-catalysis of LaH_3 and NbH during the hydrogen desorption process.

As previously discussed, the NbH + LaH_3 co-catalyzed hydride composite exhibited greater hydrogen release than the single NbH- or LaH_3-doped hydride, which demonstrates the synergistic effect between the NbH and LaH_3 additives. However, NbH-doped MgH_2 hydride exhibited the highest hydrogen absorption capacity, whereas the NbH and LaH_3 co-doped composite exhibited the second-highest hydrogen capacity. These results likely reflect particle aggregation in the co-doped samples, which can reduce the surface area of the hydride and affect the hydrogen diffusion. Because the hydrogenation process is more dependent on the diffusion rate than the dehydrogenation process, the NbH and LaH_3 co-doped hydride composite exhibits the highest hydrogen release but the second-highest hydrogen absorption capacity.

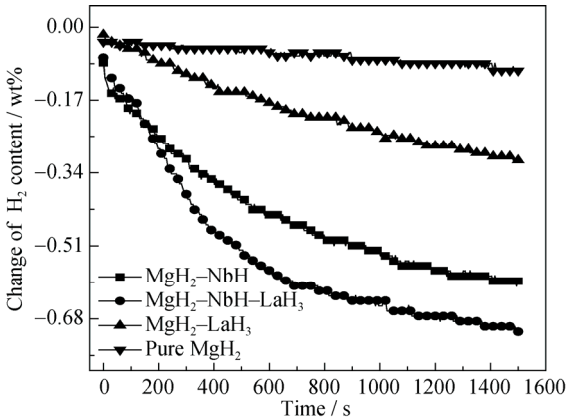

Fig. 9. Dehydriding curves for MgH_2–NbH, MgH_2–NbH–LaH_3, MgH_2–LaH_3, and pure MgH_2 at 548 K.

3.3. Determination of activation energy

A noticeable feature presented in Fig. 10 is that MgH_2–NbH–LaH_3 shows the lowest dehydriding peak temperature, which is as low as 595.03 K, or 94.26 K lower than that of pure MgH_2. The dehydriding peak temperatures of MgH_2–NbH and MgH_2–LaH_3 are 598.35 and 667.51 K, respectively. This result indicates that the additive composed of LaH_3 and NbH can reduce the hydrogen desorption temperature of MgH_2 more effectively than the single NbH or LaH_3 additive, which is likely related to the co-catalysis effect of LaH_3 and NbH.

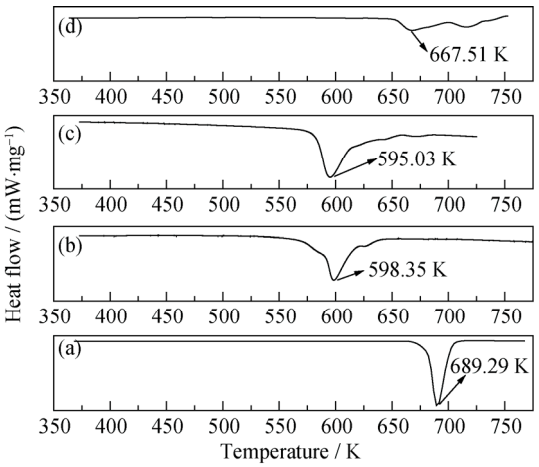

Fig. 10. DTA curves of different samples at a heating rate of 5 K/min: (a) pure MgH_2; (b) MgH_2–NbH; (c) MgH_2–NbH–LaH_3; (d) MgH_2–LaH_3.

The activation energy (E_a) of the dehydrogenation process for the samples was fitted using the Kissinger equation (Eq. (2)):

$$\ln\left(\frac{\alpha}{T_m^2}\right) = -\frac{E_a}{RT_m + \ln\left(\frac{k_0 R}{E_a}\right)} \quad (2)$$

which can be simplified to

$$\frac{d\left[\ln\left(\frac{\alpha}{T_m^2}\right)\right]}{d\left(\frac{1}{T_m}\right)} = -\frac{E_a}{R} \quad (3)$$

where α is the heating rate, T_m is the absolute temperature at the maximum desorption rate, and R is the ideal gas constant. Fig. 11 shows a plot of $\ln(T_m^2)$ versus $1000/T_m$. The dehydriding peak temperature of the samples at various heating rates and the obtained E_a values are summarized in Table 1. The E_a for the hydrogen desorption reaction of MgH_2–NbH–LaH_3 decreases to (75.70 ± 3.59) kJ·mol^{-1}, which is 47.36 kJ·mol^{-1} lower than that of pure MgH_2, whose E_a is (123.06 ± 1.24) kJ·mol^{-1}. The E_a for MgH_2–NbH is (77.14 ± 1.52) kJ·mol^{-1}. Thus, the addition of NbH resulted in a decrease of E_a during the hydrogen desorption process by decreasing the energy barrier of MgH_2.

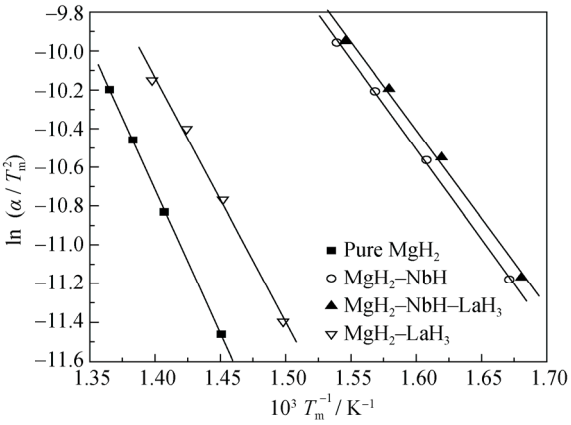

Fig. 11. Kissinger plot of the first-order dehydrogenation process of different samples at various heating rates.

Table 1. T_m and E_a corresponding to four samples

Sample	Heating rate used in DTA / (K·min^{-1})	T_m / K	E_a / (kJ·mol^{-1})
pure MgH_2	5	689.29	123.06 ± 1.24
	10	710.72	
	15	723.01	
	20	732.54	
MgH_2–NbH	5	598.35	77.14 ± 1.52
	10	621.94	
	15	637.56	
	20	649.68	
MgH_2–NbH–LaH_3	5	595.03	75.70 ± 3.59
	10	617.52	
	15	633.26	
	20	646.95	
MgH_2–LaH_3	5	667.51	104.81 ± 5.34
	10	688.72	
	15	702.19	
	20	715.43	

4. Conclusions

A composite of MgH_2 + 10wt%LaH_3 + 10wt%NbH was prepared by mechanical milling. This composite released 0.67wt% H_2 within 20 min at 548 K. By contrast, pure MgH_2 and MgH_2 doped separately with LaH_3 and NbH released only 0.1wt%, 0.28wt%, and 0.57wt% H_2, respectively. These results reveal that the LaH_3 and NbH additive can

improve the properties of MgH_2 because of the synergistic catalysis effect. The dehydriding peak temperature of the composite was reduced to 595.03 K, 94.26 K lower than that of pure MgH_2. The E_a of the dehydrogenation process of MgH_2 decreased from 123.06 to 75.70 $kJ \cdot mol^{-1}$ after it was mechanically milled together with LaH_3 and NbH. Microstructure measurements revealed that the particle size of the composite was remarkably decreased and that La and Nb were homogeneously distributed in the matrix, providing more diffusion paths and shortening the diffusion pathway for hydrogen atoms in the composite.

Acknowledgements

This work was financially supported by the National Natural Science Foundation of China (Nos. 50971112 and 51471065) and the Scientific Research Projects in Colleges and Universities in Hebei Province, China (ZD2014004).

References

[1] D. Mori and K. Hirose, Recent challenges of hydrogen storage technologies for fuel cell vehicles, *Int. J. Hydrogen Energy*, 34(2009), No. 10, p. 4569.

[2] L.C. Pei, S.M. Han, J.S. Wang, L. Hu, X. Zhao, and B.Z. Liu, Hydrogen storage properties and phase structures of RMg_2Ni (R = La, Ce, Pr, Nd) alloys, *Mater. Sci. Eng. B*, 177(2012), No. 18, p. 1589.

[3] B. Sakintuna, F. Lamari-Darkrim, and M. Hirscher, Metal hydride materials for solid hydrogen storage: A review, *Int. J. Hydrogen Energy*, 32(2007), No. 9, p. 1121.

[4] W. Zhao, V. Fierro, N. Fernández-Huerta, M.T. Izquierdo, and A. Celzard, Impact of synthesis conditions of KOH activated carbons on their hydrogen storage capacities, *Int. J. Hydrogen Energy*, 37(2012), No. 19, p. 14278.

[5] M. Au, Hydrogen storage properties of magnesium based nanostructured composite materials, *Mater. Sci. Eng. B*, 117(2005), No. 1, p. 37.

[6] H.W. Dong, L.Z. Ou Yang, T. Sun, and M. Zhu, Effect of ball milling on hydrogen storage of Mg_3La alloy, *J. Rare Earths*, 26(2008), No. 2, p. 303.

[7] M. Abdellatief, R. Campostrini, M. Leoni, and P. Scardi, Effects of SnO_2 on hydrogen desorption of MgH_2, *Int. J. Hydrogen Energy*, 38(2013), No. 11, p. 4664.

[8] P. Pei, X.P. Song, J. Liu, A.N. Song, P.L. Zhang, and G.L. Chen, Study on the hydrogen desorption mechanism of a Mg–V composite prepared by SPS, *Int. J. Hydrogen Energy*, 37(2012), No. 1, p. 984.

[9] J.R. Ares, F. Leardini, P. Díaz-Chao, J. Bodega, D.W. Koon, I.J. Ferrer, J.F. Fernández, and C. Sánchez, Hydrogen desorption in nanocrystalline MgH_2 thin films at room temperature, *J. Alloys Compd.*, 495(2010), No. 2, p. 650.

[10] L.P. Ma, P. Wang, and H.M. Cheng, Improving hydrogen sorption kinetics of MgH_2 by mechanical milling with TiF_3, *J. Alloys Compd.*, 432(2007), No. 1-2, p. 1.

[11] M. Zhu, Y.S. Lu, L.Z. Ouyang, and H. Wang, Thermodynamic tuning of Mg-based hydrogen storage alloys: a review, *Materials*, 6(2013), No. 10, p. 4654.

[12] M. Tian and C.X. Shang, Effect of TiC and Mo_2C on hydrogen desorption of mechanically milled MgH_2, *J. Chem. Sci. Technol.*, 1(2012), p. 54.

[13] H. Wang, S.F. Zhang, J.W. Liu, L.Z. Ou Yang, and M. Zhu, Enhanced dehydrogenation of nanoscale MgH_2 confined by ordered mesoporous silica, *Mater. Chem. Phys.*, 136(2012), No. 1, p. 146.

[14] D.W. Zhou, P. Peng, J.S. Liu, L. Chen, and Y.J. Hu, First-principles study on structural stability of 3d transition metal alloying magnesium hydride, *Trans. Nonferrous Met. Soc. China*, 16(2006), No. 1, p. 23.

[15] M.D. Riktor, S. Deledda, M. Herrich, O. Gutfleisch, H. Fjellvåg, and B.C. Hauback, Hydride formation in ball-milled and cryomilled Mg–Fe powder mixtures, *Mater. Sci. Eng. B*, 158(2009), No. 1-3, p. 19.

[16] S. Milošević, Z. Rašković-Lovre, S. Kurko, R. Vujasin, N. Cvjetićanin, L. Matović, and J.G. Novaković, Influence of VO_2 nanostructured ceramics on hydrogen desorption properties from magnesium hydride, *Ceram. Int.*, 39(2013), No. 1, p. 51.

[17] Y.H. Jia, S.M. Han, W. Zhang, X. Zhao, P.F. Sun, Y.Q. Liu , H. Shi, and J.S. Wang, Hydrogen absorption and desorption kinetics of MgH_2 catalyzed by MoS_2 and MoO_2, *Int. J. Hydrogen Energy*, 38(2013), No. 5, p. 2352.

[18] S.A. Jin, J.H. Shim, Y.W. Cho, and K.W. Yi, Dehydrogenation and hydrogenation characteristics of MgH_2 with transition metal fluoride, *J. Power Sources*, 172(2007), No. 2, p. 859.

[19] I.E. Malka, M. Pisarek, T. Czujko, and J. Bystrzycki, A study of the ZrF_4, NbF_5, TaF_5, and $TiCl_3$ influences on the MgH_2 sorption properties, *Int. J. Hydrogen Energy*, 36(2011), No. 20, p. 12909.

[20] R.K. Singh, T. Sadhasivam, G.I. Sheeja, P. Singh, and O.N. Srivastava, Effect of different sized CeO_2 nano particles on decomposition and hydrogen absorption kinetics of magnesium hydride, *Int. J. Hydrogen Energy*, 38(2013), No. 14, p. 6221.

[21] R. Gupta, F. Agresti, S.L. Russo, A. Maddalena, P. Palade, and G. Principi, Structure and hydrogen storage properties of MgH_2 catalysed with La_2O_3, *J. Alloys Compd.*, 450(2008),

No. 1-2, p. 310.

[22] R.R. Shahi, A.P. Tiwari, M.A. Shaz, and O.N. Srivastava, Studies on de/rehydrogenation characteristics of nanocrystalline MgH_2 co-catalyzed with Ti, Fe and Ni, *Int. J. Hydrogen Energy*, 38(2013), No. 6, p. 2778.

[23] H. Wang, H.J. Lin, W.T. Cai, L.Z. Ou Yang, and M.S. Zhu, Tuning kinetics and thermodynamics of hydrogen storage in light metal element based systems—a review of recent progress, *J. Alloys Compd.*, 658(2016), p. 280.

[24] X.Z. Xiao, C.C. Xu, J. Shao, L.T. Zhang, T. Qin, S.Q. Li, H.W. Ge, Q.D. Wang, and L.X. Chen, Remarkable hydrogen desorption properties and mechanisms of the Mg_2FeH_6@MgH_2 core–shell nanostructure, *J. Mater. Chem. A*, 3(2015), No. 10, p. 5517.

[25] H. Xue, X.Z. Xiao, J. Shao, B. Zhai, X.L. Fan, C.J. Cheng, S.Q. Li, H.W. Ge, Q.D. Wang, and L.X. Chen, Building robust architectures of carbon wrapped transition metal nanoparticles toward high-catalytic enhancement of $2LiBH_4$–MgH_2 system for hydrogen storage cycling performances, *Nanoscale*, 8(2016), p. 14898.

[26] K. Wang, H.F. Du, Z.Y. Wang, M.X. Gao, H.G. Pan, and Y.F. Liu, Novel MAX-phase Ti_3AlC_2 catalyst for improving the reversible hydrogen storage properties of MgH_2, *Int. J. Hydrogen Energy*, 42(2017), p. 4244.

[27] Y.F. Liu, H.F. Du, X. Zhang, Y.X. Yang, M.X. Gao, and H.G. Pan, Superior catalytic activity derived from a two-dimensional Ti_3C_2 precursor towards the hydrogen storage reaction of magnesium hydride, *Chem. Commun.*, 52(2016), No. 4, p. 705.

[28] X.Z. Xiao, Z. Liu, S.S. Yarahmadi, and D.H. Gregory, Facile preparation of β-/γ-MgH_2 nanocomposites under mild conditions and pathways to rapid dehydrogenation, *Phys. Chem. Chem. Phys.*, 18(2016), No. 15, p. 10492.

[29] Y. Li, Y. Tao, and Q. Huo, Effect of stoichiometry and Cu-substitution on the phase structure and hydrogen storage properties of Ml–Mg–Ni-based alloys, *Int. J. Miner. Metall. Mater.*, 22(2015), No. 1, p. 86.

[30] X.L. Zhu, L.C. Pei, Z.Y. Zhao, B.Z. Liu, S.M. Han, and R.B. Wang, The catalysis mechanism of La hydrides on hydrogen storage properties of MgH_2 in MgH_2 + *x*wt% LaH_3 (*x* = 0, 10, 20, and 30) composites, *J. Alloys Compd.*, 577(2013), p. 64.

[31] X. Zhao, S.M. Han, Y. Li, X.C. Chen, and D.D. Ke, Effect of $CeH_{2.29}$ on the microstructures and hydrogen properties of $LiBH_4$–Mg_2NiH_4 composites, *Int. J. Miner. Metall. Mater.*, 22(2015), No. 4, p. 423.

[32] M.O.T. da Conceição, M.C. Brum, D.S. dos Santos, and M.L. Dias, Hydrogen sorption enhancement by Nb_2O_5 and Nb catalysts combined with MgH_2, *J. Alloys Compd.*, 550(2013), p. 179.

[33] S.A. Jin, J.H. Shim, J.P. Ahn, Y.W. Cho, and K.W. Yi, Improvement in hydrogen sorption kinetics of MgH_2 with Nb hydride catalyst, *Acta Mater.*, 55(2007), No. 15, p. 5073.

[34] L.T. Zhang, X.Z. Xiao, C.C. Xu, J.G. Zheng, X.L. Fan, J. Shao, S.Q. Li, H.W. Ge, Q.D. Wang, and L.X. Chen, Remarkably improved hydrogen storage performance of MgH_2 catalyzed by multi-valence NbH*x* nanoparticles, *J. Phys. Chem. C*, 119(2015), No. 16, p. 8554.